On the relevance of the atomic-scale contact potential difference by Amplitude modulation- and Frequency modulation-Kelvin probe force microscopy

Laurent Nony, Franck Bocquet, Christian Loppacher, Thilo Glatzel

▶ **To cite this version:**

Laurent Nony, Franck Bocquet, Christian Loppacher, Thilo Glatzel. On the relevance of the atomic-scale contact potential difference by Amplitude modulation- and Frequency modulation-Kelvin probe force microscopy. Nanotechnology, 2009, 20, pp.264014. 10.1088/0957-4484/20/26/264014 . hal-00401595

HAL Id: hal-00401595
https://hal.science/hal-00401595

Submitted on 16 Jul 2009

HAL is a multi-disciplinary open access archive for the deposit and dissemination of scientific research documents, whether they are published or not. The documents may come from teaching and research institutions in France or abroad, or from public or private research centers.

L'archive ouverte pluridisciplinaire **HAL**, est destinée au dépôt et à la diffusion de documents scientifiques de niveau recherche, publiés ou non, émanant des établissements d'enseignement et de recherche français ou étrangers, des laboratoires publics ou privés.

Published in Nanotechnology **20**, 264014 (2009)
doi:10.1088/0957-4484/20/26/264014

On the relevance of the atomic-scale contact potential difference by Amplitude modulation- and Frequency modulation-Kelvin probe force microscopy

Laurent Nony[1,2,*], Franck Bocquet[1,2], and Christian Loppacher[1,2]

[(1)] *Aix-Marseille Université, IM2NP,*
Centre Scientifique de Saint-Jérôme,
Avenue Escadrille Normandie-Niemen, Case 151,
F-13397 Marseille CEDEX 20, France

[(2)] *CNRS, IM2NP (UMR 6242), F-13397 Marseille-Toulon, France*

Thilo Glatzel

Department of Physics, University of Basel,
Klingelbergstr. 82, CH-4056 Basel, Switzerland

(Dated: July 16, 2009)

* To whom correspondence should be addressed; E-mail: laurent.nony@im2np.fr.

Abstract

The influence of short-range electrostatic forces on the measured local Contact Potential Difference (CPD) by means of Amplitude Modulation- and Frequency Modulation-Kelvin Probe Force Microscopy (AM- and FM-KPFM) is discussed on the base of numeric and analytic descriptions of both methods. The goal of this work is to help interpreting recent experimental results reporting atomically-resolved CPD images, in particular on bulk insulating samples. The discussion is carried out on the base of spectroscopic curves. The expression of the bias-dependent electrostatic force derives from a previous work and is estimated between a tip with simple geometry and the (001) facet of a perfect alkali halide single crystal. The force, with a short-range character, scales as a second-order polynomial function of the bias voltage. It is stated that the linear term is responsible for the occurrence of the atomic-scale CPD contrast, while the quadratic one, involving the sample polarisation, accounts for the detected signal by the KPFM methods. Nevertheless, analytic and numeric approaches stress the influence of the linear term on the measured CPD which intrinsically hinders the possibility to perform quantitative CPD measurements, but also makes the measured "pseudo-CPD" strongly deviating from the surface potential. Hence, in the short-range regime, AM- or FM-KPFM measurements neither reflect the CPD nor the local surface potential, but rather an effective value which is convoluted by the geometric parameters of the tip, the so-called local CPD. It is also stated that the local CPD measured by means of AM- or FM-KPFM differs when sub-nanometer vibration amplitudes of the cantilever are used. Otherwise, AM- and FM-KPFM measurements should be almost similar. At last, the influence of long-range, capacitive, electrostatic forces is discussed in conjunction with the short-range ones. This allows us to draw conclusions regarding the distance dependence of the local CPD which then exhibits a resonant behavior as a function of the tip-surface separation. This phenomenon is expected to play a role in the KPFM imaging process.

I. INTRODUCTION

Kelvin Probe Force Microscopy (KPFM) is a scanning probe method[1] which is based on the detection and the dynamic compensation of the electrostatic forces occurring between a nano-tip and a sample when they are electrically connected. These forces stem from intrinsic work function differences between the tip and the sample surface[2,3], capacitive contributions, as well as from trapped charges at the tip apex and/or the surface upon preparation procedures[4]. The KPFM method actually provides access to the contact potential difference (CPD)[5], *i.e.* the work function of the sample referenced to the work function of the tip: $qV_{cpd} = \Delta\phi = \phi_{tip} - \phi_{sample}$, q being the elementary electrical charge.

The technique is based on the regular noncontact-Atomic Force Microscopy (nc-AFM) operating mode, which is strongly sensitive to electrostatic forces. Two KPFM-based techniques provide facilities to map the spatial variations of the CPD on the nanometer scale, namely Amplitude Modulation-KPFM (AM-KPFM, refs.[6,7]) or Frequency Modulation-KPFM (FM-KPFM, ref.[8]). The connection between KPFM and nc-AFM has brought a complimentary information to the usual topography and more controversial dissipation (so-called damping) channels, and has already been used to map the chemical identity of surface atoms[9]. KPFM early proved its ability to map the spatial variations of the CPD on the nanometer scale with a resolution of few mV[6,10,11]. Different groups reported atomically-resolved CPD images, some including even the influence of atomic adsorbates[8,9,12,13,14,15]. More recently, the CPD atomic-scale contrast was reported on metallic and ionic thin films on InSb[16], on oxides[17,18] and on ionic bulk insulating surfaces[19]. The former results suggest that, very close to the surface, the CPD rather has a local character[20]. Among the former references however, despite the consistency between the lateral periodicity of the local CPD images and the surface lattice constant, the values rarely fit to the CPD values reported by other experimental methods or with the theoretical predictions[8,12,14]. For instance, on the complex Si(111)$5\sqrt{3} \times 5\sqrt{3}$-Sb surface, Okamoto *et al.* concluded that the CPD images mainly reflect the electrostatic force distribution on the surface rather than the work functions distribution[9,15]. It has also been mentioned that the measured CPD was dependent on the tip-surface distance[15,16,21]. Thus, a cross-talk between the topography and CPD images is very likely, as soon as the topography feedback circuit is engaged.

These results make the interpretation of the CPD atomic-scale contrast difficult to explain

and the measurements ultimately questionable. Besides, the CPD being intrinsically a macroscopic property of the tip-surface system, there is currently an intense debate dealing with the apparent contradiction between *CPD* and *local CPD* measurements, which actually raises the questions of the origin and the reliability of atomic-scale resolution in KPFM[16,18,19].

The difficulty for interpreting the experimental results stems from the lack of theoretical description for the short-range electrostatic forces which are intricately involved in the atomic-scale contrast and the way these forces are processed by the KPFM control electronics. In order to address these questions, we first have focussed on the CPD atomic-scale contrast reported experimentally on the KBr(001) insulating surface[19]. In this preliminary work, an analytic model for the short-range electrostatic interaction between a biased tip and the KBr surface was developed.

In the present work, the influence of such a short-range electrostatic force on the measured local CPD is discussed by means of a numerical implementation of the AM-KPFM and FM-KPFM setups within our nc-AFM simulator[22]. The numerical results are completed with an analytical approach providing approximated expressions of the modulated components used by the AM- and FM-KPFM methods as a function of the DC bias voltage. The following section reminds the AM- and FM-KPFM setups, their operational mode and their experimental implementation, which were accurately duplicated on the numerical level. In section III, the analytical model for the short-range electrostatic force is briefly introduced and we stress the influence of the dynamic polarisation of the ionic crystal, which is for a large part responsible for the occurrence of the atomic contrast. In sections IV A and IV B, the analytic and numeric approaches are discussed in respect with the CPD atomic-scale contrast. In section V, we extend the framework of the atomic-scale CPD contrast to long-range electrostatic forces. This allows us to draw conclusions regarding the distance dependence of the local CPD, which is not possible when considering uniquely short-range electrostatic forces.

II. AM- AND FM-KPFM EXPERIMENTAL METHODS

KPFM relies on the dynamic compensation of the electrostatic forces arising between the tip and the sample, hereafter referred to as the electrodes. For that purpose, an amplitude modulation technique is used. The electrostatic force is triggered when modulating the bias

voltage which is applied between the electrodes:

$$V_b(t) = V_{DC} + V_{mod}\cos(2\pi f_{mod}t) \tag{1}$$

When dealing with metallic electrodes and for large tip-surface distances compared to atomic dimensions, the electrostatic part of the total force can be written as:

$$F_{es}(t) = -\frac{1}{2}\frac{\partial \mathcal{C}(z)}{\partial z}(V_b(t) \pm V_{cpd})^2, \tag{2}$$

$\mathcal{C}(z)$ being the expression of the tip-surface capacitor, influenced by the geometry of both electrodes[23,24]. The $\pm$ sign depends upon the bias voltage is applied to the tip or to the sample. When applied to the tip (sample grounded), the measured DC potential is the opposite of the CPD, hence one should write $V_b(t) + V_{cpd}$, otherwise the opposite (tip grounded). In the following, we will assume that the tip is grounded and will write $V_b(t) - V_{cpd}$.

The above expression of the force gives three temporal components, the first one being static, the second and third ones being amplitude-modulated at f_{mod} and $2f_{mod}$, respectively. The relevant component for the KPFM technique is the one modulated at f_{mod}:

$$F_{es}^{f_{mod}}(t) = \frac{\partial \mathcal{C}(z)}{\partial z}(V_{DC} - V_{cpd})V_{mod}\cos(2\pi f_{mod}t) \tag{3}$$

This component is fed into a dual phase lock-in amplifier (LIA) which detects the amplitude of the signal, A_K, from the measurement of the in-phase and out-of-phase components X and Y, respectively. The signal X is then injected into a proportional/integral controller, the output of which supplies the proper DC bias voltage to minimize, or ideally cancel X and hence A_K, *i.e.* also $F_{es}^{f_{mod}}$ (*cf.* equ.3). It is important to notice that X is supposed to be used instead of A_K in the Kelvin controller, because it can become negative and thereby handle negative error signals, while A_K not. Thus, according to equ.3, the output of the controller is the DC bias which compensates the CPD: $V_{DC}^{(c)} = +V_{cpd}$.

The experimental implementation can be done in two ways, both of them relying on the detection and subsequent cancellation of A_K, but differing regarding the signal that carries the modulation. In FM-KPFM, the modulation is performed at a few kHz and detected in the frequency shift signal (Δf) provided by the phase-locked-loop[25] (PLL). In AM-KPFM, the modulation frequency matches the second flexural eigenmode of the cantilever[7,26], with typical frequency[27]: $f_1 \simeq 6.24 f_0$. The experimental setups have been depicted in fig.1. They

are based on the well-established nc-AFM operating mode which relies on the PLL-controlled excitation of the cantilever[22,28].

Equs.2 and 3 show that the KPFM methods intricately relies on *electrostatic forces scaling quadratically with the bias voltage*, otherwise no CPD contrast would be detected by the experimental method. Besides, atomically-resolved CPD images testify that these forces have a short-range character. However, equ.2 is improper to describe this contrast, first because the distance dependence, *i.e.* the expression of the tip-surface capacitor, has usually not a short-range character and second because this expression derives from a classical electrostatic approach between continuous-like metallic bodies and hence does not take into account atomic fluctuations of the surface potential of the insulating sample. Another fundamental aspect of the problem stems from the influence of the technique onto the measured CPD. In our previous work[19] as well as in the work by Krok *et al.*[16], there are strong evidences that short-range electrostatic forces scale not only quadratically, but also linearly with the applied bias voltage. Assuming a linear term in equ.2: $F_{es} = C_2(V_b(t) - V_{cpd})^2 + C_1(V_b(t) - V_{cpd})$, then the modulated component of the force is modified consistently: $F_{es}^{f_{mod}} = [C_1 + 2C_2(V_{DC} - V_{cpd})]V_{mod}\cos(2\pi f_{mod}t)$. The compensated CPD becomes: $V_{DC}^{(c)} = V_{cpd} - C_1/(2C_2)$, which fakes its physical content. The physics that it carries now differs from the actual CPD and depends on the coefficients C_1 and C_2. Obviously, this remains true when other power laws of the bias are to be considered in the expression of the electrostatic force.

III. SHORT-RANGE ELECTROSTATIC FORCE MODEL

In ref.[19], Bocquet *et al.* proposed an analytical approach to the short-range electrostatic force between a nanoscopic tip and the (001) surface of a perfect alkali halide single crystal of KBr, *i.e.* not including residual net charges. The sample is several millimeters high, which places the metallic counter-electrode far from the tip in comparison with other setups. The two former assumptions insure that no Coulombic nor capacitive long-range electrostatic forces act onto the tip in the process that is being discussed. The tip consists of two embedded half-spheres with different radii. The bigger radius R stands for the mesoscopic body of the tip ($R \simeq 5$ nm). The sphere with radius $R_a \ll R$, which is half-embedded within the macroscopic body, rather stands for a microscoscopic nanoasperity supposed to

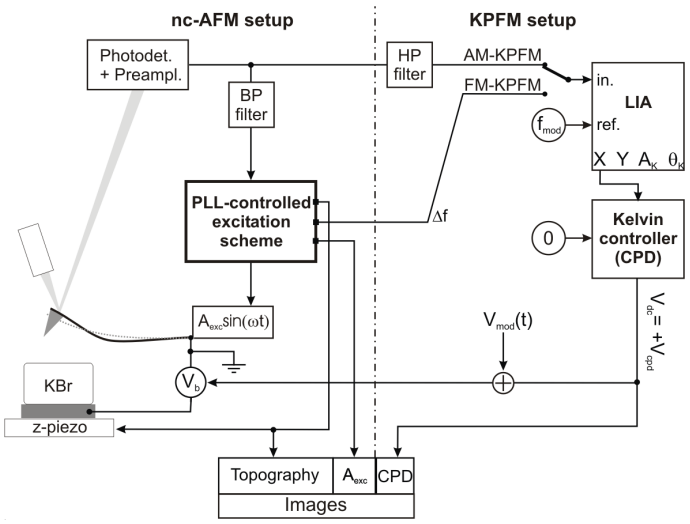

FIG. 1: Scheme of the combined nc-AFM / KPFM experimental setup which was duplicated numerically. AM- or FM-KPFM mode is selected upon the position of the switch. The PLL-controlled excitation scheme was detailed in ref.[22].

favor the occurrence of the atomic-scale contrast ($R_a \simeq 1$ Å, *cf.* fig.2a). With this simple geometry, the expression of the force can be split into two major contributions:

$$F_{es}(V_b, z) = F^{(1)}_{m\mu} + F^{(2)}_{\mu} = C_1(V_b(t) - V_{cpd})e^{-\alpha z} + [C_0 + C_2(V_b(t) - V_{cpd})^2]e^{-2\alpha z}, \quad (4)$$

α is a coefficient which scales with the lattice constant of the crystal, a, according to $\alpha = 2\sqrt{2}\pi/a$. The coefficients C_0, C_1 and C_2 are written:

$$C_0 = -\frac{R^2 q^2}{2\epsilon_0 a'^4} A^{(2)} e^{-2\alpha R_a} \text{ and } C_2 = 2C_0 \left(\frac{2\pi\chi_d}{a' q R}\right)^2 \quad (5)$$

and:

$$C_1 = -\frac{3R_a^2 q \widetilde{\epsilon}_d}{a'^2 R} D^{(1)} e^{-\alpha R_a} [\cos(\widetilde{x}_0) + \cos(\widetilde{y}_0)] \quad (6)$$

R and R_a are the tip's radii defined above. ϵ_0, $\widetilde{\epsilon}_d$ and χ_d are the vacuum dielectric permittivity, KBr effective dielectric permittivity and KBr dielectric susceptibility, respectively. In the former reference, we had set: $\widetilde{\epsilon}_d = 4.38$ and $\chi_d = 9\ 10^{-39}$ Fm^2. $A^{(2)}$ and $D^{(1)}$ are two numeric coefficients depending on the values of radii R and R_a in a complex manner (*cf.* equs.A2 and A6 in ref.[19]). $\widetilde{x}_0 = 2\pi x_0/a'$ and $\widetilde{y}_0 = 2\pi y_0/a'$ are the reduced coordinates of

the position of the tip onto the KBr(001) surface. Setting $x_0 = y_0 = 0$ or $x_0 = y_0 = a'/2$ locates the tip on top of an anion or of a cation, respectively. Thus, the coefficient C_1 carries the lateral modulation of the force over the crystal surface.

$F_{m\mu}^{(1)}$ depicts the coupling between the microscopic structure of the tip apex and the capacitor consisting of the tip, the ionic crystal and the counter-electrode. It originates from the influence of the KBr Madelung surface potential (MSP) onto the surface charge density that develops within the microscopic nanoasperity due to the bias voltage V_b. $F_{\mu}^{(2)}$, depicts the influence of the MSP onto the mesoscopic part of the tip, independently from its microscopic structure. The exponential distance dependence, which stems from the MSP, shows that the force has a short-range character. $F_{m\mu}^{(1)}$ has the lateral periodicity of the MSP (*cf.* coefficient C_1), whereas $F_{\mu}^{(2)}$ exhibits no spatial dependence and merely acts as a static component, which shifts the total force. Therefore the CPD atomic-scale contrast is mainly carried by the term $F_{m\mu}^{(1)}$. The total force is in the range of ten pico-Newtons. Let us finally note that the quadratic bias voltage dependence of $F_{\mu}^{(2)}$ occurs if and only if the ionic polarisation of the sample due to the influence of the tip/counter-electrode capacitor is explicitly considered. By ionic polarisation, it is meant a net vertical displacement of the ions from their equilibrium positions within the crystal upon their sign, which changes the strength of the MSP[29]. This displacement follows the bias modulation dynamically.

The above elements allow us to draw two major conclusions: (1)- the measurement of the local CPD by means of KPFM is partly made possible *via* the ionic polarisation of the sample (required quadratic bias voltage dependence) and (2)- the occurrence of the atomic-scale contrast, indeed consistent with the ionic positions, relies on a linear bias voltage dependence of the short-range electrostatic force. Therefore, according to the discussion of section II, it is expected that the compensated CPD, either measured by AM- or FM-KPFM, does not match the actual tip-surface CPD.

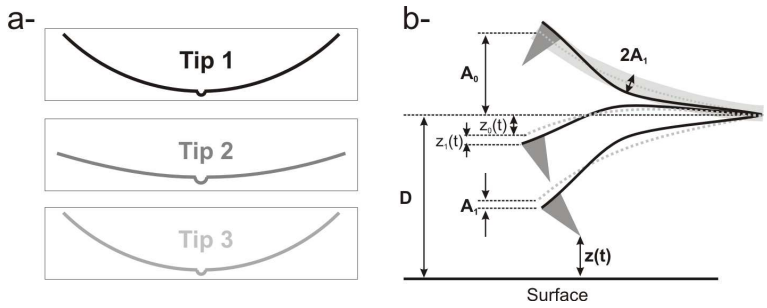

FIG. 2: a- Schemes of the three tips used for the analytic and numeric calculations, properly scaled. The set of parameters (R, R_a) in Å are: tip1(50, 1); tip2(120, 1.5); tip3(50, 1.1). For the analytic calculations, the sets of coefficients $(A^{(2)}, D^{(1)})$ are: tip1(-2.5,-15); tip2(-1.1,-25); tip3(-2.5,-20). b- Scheme of the vibration of the cantilever at the 1^{st} and 2^{nd} eigenmodes, corresponding to instantaneous positions $z_0(t)$ and $z_1(t)$, respectively. The instantaneous tip-surface separation is $z(t) = D - z_0(t) - z_1(t)$.

IV. ANALYTIC AND NUMERIC APPROACHES

A. AM-KPFM

1. *Analytic approach*

In ref.[19], a self-consistent approximated expression of the vibration amplitude of the second flexural eigenmode of the cantilever was proposed. Let $z_1(t)$ be the instantaneous deflection of this mode (*cf.* fig.2b) and A_1 its vibration amplitude. It is ruled by the nonlinear equation of motion:

$$\ddot{z_1}(t) + \frac{\omega_1}{Q_1}\dot{z_1}(t) + \omega_1^2 z_1(t) = \frac{F_{ext}}{m_1} + \frac{F_{es}(V_b, z)}{m_1}, \tag{7}$$

where Q_1, $\omega_1 = 2\pi f_1$ and m_1 are the quality factor, the resonance pulsation and the effective mass of the mode, respectively. F_{ext} stands for the actuation force of the fundamental flexural mode of the cantilever (resonance frequency f_0). The resonance amplitude of this mode is A_0. Owing to the large difference between f_0 and f_1, F_{ext} does not influence $z_1(t)$. Let $z_0(t)$ be the instantaneous position of the fundamental mode. Thus, the instantaneous tip-surface separation to be considered for $F_{es}(V_b, z)$ is: $z(t) = D - z_0(t) - z_1(t)$, D being the separation between the surface and the equilibrium position of the cantilever at rest (*cf.*

fig.2b). Owing to the exponential distance-dependence of $F_{es}(V_b, z)$, the second mode is not actuated harmonically, but rather stepwise-like upon $z(t)$. This makes the structure of the actuation of the second mode rather complex, but nevertheless enough to permit the development of the steady state, which merely stems from the large value of Q_1 (a few thousands).

When linearizing equ.7 with respect to $z_1(t)$ and assuming it as harmonic, an approximate expression for A_1 can be derived (*cf.* ref.[19] for details):

$$A_1 = l_0 \frac{\sqrt{(l_3 - l_2)^2 + l_1^2}}{l_1^2 + l_2^2 - l_3^2} \tag{8}$$

Except l_0, coefficients l_1, l_2 and l_3 are reported in the appendix. l_0 is written:

$$l_0 = \frac{C_1 a_0}{m_1} e^{-\alpha z_{min}} V_{mod} + 2\frac{C_2 b_0}{m_1} e^{-2\alpha z_{min}} (V_{DC} - V_{cpd}) V_{mod} \tag{9}$$

$z_{min} = D - A_0$ stands for the minimum tip-surface separation, *i.e.* at the lower turning point of the tip when neglecting A_1 with respect to A_0, which is practically always correct (see below). a_0 and b_0 are the the zero-order Fourier coefficients of the functions $\exp\{-\alpha A_0[1 - \cos(2\pi f_0 t)]\}$ and $\exp\{-2\alpha A_0[1 - \cos(2\pi f_0 t)]\}$ that occur in the expression of the force when expanding $z(t)$. The n$^{\text{th}}$ Fourier coefficients are: $a_n = 2\exp(-\alpha A_0) I(n, \alpha A_0)$ and $b_n = 2\exp(-2\alpha A_0) I(n, 2\alpha A_0)$, I being the modified function of Bessel of the first kind[19]. Hence, the condition on the bias to nullify A_1, *i.e.* the modulated component at f_{mod} in AM-KPFM, is simply $l_0 = 0$, which yields:

$$V_{DC}^{(c)} = V_{cpd} - \frac{C_1}{2C_2} \frac{a_0}{b_0} e^{+\alpha z_{min}} \tag{10}$$

The above expression shows that the compensated CPD has the lateral periodicity of the MSP (coefficient C_1). However, it also depends on the tip parameters R and R_a. This result shows that the experimental measurements of the local CPD by AM-KPFM neither reflects the actual tip-surface CPD, nor the value of the local surface potential, but rather an effective value that is convoluted by the tip geometry. This originates from the linear bias dependence in the expression of the force, as stated before. Nevertheless, the lateral periodicity of the MSP is preserved in the CPD contrast, which makes CPD differential measurements among atomic sites reliable.

Equ.10 shows that, above an anion, the compensated CPD becomes more and more negative as the tip-surface separation is increased[30]. This rather surprising behavior stems from the faster distance dependence of $F_{\mu}^{(2)}$ compared to $F_{m\mu}^{(1)}$, as discussed in ref.[19]. Therefore, the distance dependence of the compensated local CPD depends much on the tip geometry. Obviously, this behavior cannot stand for any tip-surface separation owing to the exponential decay of the short-range electrostatic force which triggers the motion of the cantilever's 2nd eigenmode and hereby, the detection of the local CPD. If the force is too weak, no CPD can be detected anymore. However, within a narrow range of tip-surface separations, typically a few angströms, it might be detectable.

Nevertheless, the above discussion is not complete because it is insufficient to consider the short-range electrostatic force as the main triggering source of the cantilever since it is known that long-range capacitive forces always occur on the experimental level. In section V, the distance dependence of the local CPD is discussed in more detail within the framework of short- and long-range electrostatic interactions.

2. Numeric approach

The numerical implementation of the AM-KPFM setup has been performed within the code of the nc-AFM simulator. In particular, although the resonance frequency of the second flexural mode is in the MHz range ($f_1 = 6.24 f_0 = 6.24 \times 150$ kHz $\simeq 940$ kHz), we have kept the sampling frequency standing for the analog parts of the electronics constant, namely $f_{s_2} = 400$ MHz (*cf.* ref.[22] for details). This is still sufficient to integrate the differential equation of motion of the mode with an error kept low enough. The implementation sticks to the experimental setup shown in fig.1. We have used a simple first-order, high-pass filter with a 200 kHz cutoff frequency. The dual-phase LIA has a 10 kHz bandwidth. The numerical implementation is similar to the one used in the nc-AFM simulator for monitoring the phase lag between the excitation and the cantilever's response. It provides $A_K = 2\sqrt{X^2 + Y^2}$, which in the case of the AM-KPFM matches A_1, the vibration amplitude of the second eigenmode. The Kelvin controller has a 2.5 kHz bandwidth. It is a standard proportional and integral controller, the implementation of which is similar to the distance and amplitude controllers. In the present work, we merely have focussed at A_1 *vs.* V_{DC} curves, so-called spectroscopic curves. Therefore, the measurements are performed at a single (x, y) position

and the Kelvin controller is not engaged. The determination of the influence of the Kelvin controller to the measured local CPD will be addressed in a future work.

At each time step, the code integrates the differential equation for the second flexural mode (equ.7) in parallel to the equation of motion for the fundamental flexural eigenmode, which has the same form. The PLL-excitation scheme ensures that the latter mode is continuously actuated at its resonance frequency which shifts as the tip is brought closer to the surface. According to equ.4, the two equations of motion are nonlinear and coupled *via* the instantaneous separation between the tip and the surface $z(t)$ defined before.

In order to focus on the origin of the local CPD, no additional forces like long-range Van der Waals or electrostatic ones, or short-range chemical ones, have been included in the simulations. Hence, the cantilever dynamics is merely influenced by the electrostatic short-range force field. The force field is implemented as a 2D lookup table with the z variations sampled every 2 pm and bias voltage variations every 10 mV, the boundary values being adjustable upon needs. The sequence of simulation of an AM-KPFM spectroscopic curve is the following: the cantilever steady state is calculated at a tip-surface separation for which the interaction is zero and with $V_{DC} = 0$ V. The PLL and amplitude controller are then engaged and their parameters set optimally[22]. Then, the approach is performed down to an arbitrary value of z_{min}. During the approach, the second mode undergoes a frequency shift owing to the influence of the nonlinear interaction, like the first one. But it is important to ensure the on-resonance excitation of this eigenmode too. This requires to tune precisely the modulation frequency of the bias to recover the on-resonance excitation. Finally, the A_1 *vs.* V_{DC} spectroscopic curve is acquired by continuously sweeping the DC part of the bias, first from 0 down to negative values and then upwards.

3. Results and discussion

Analytic and numeric curves are reported in fig.3. The set of parameters used to perform the calculations are consistent with the experimental conditions reported in[19]: fundamental eigenmode: $f_0 = 150$ kHz, $k_0 = 30$ N/m and $Q_0 = 30000$; second eigenmode: $f_1 = 936$ kHz, $k_1 = 1168$ N/m, $Q_1 = 8000$. The modulation amplitude of the bias is $V_{mod} = 3$ V. The oscillation amplitude of the fundamental eigenmode is $A_0 = 4$ nm (8 nm peak to peak). The curves have been computed for the three tips defined in fig.2a at $z_{min} = 3$ Å , on top of an

	Tip 1	Tip 3
AM-KPFM Analytic	-1.6	-2.95
Numeric	-2.6	-6.5
FM-KPFM Analytic	-1.3	-2.4
Numeric	-2.3	-5.3

TABLE I: Comparison between analytic and numeric values of the local CPD (in volts) for tips 1 and 3 upon the KPFM method. The values have been estimated for $z_{min} = 3$ Å above an anion of the KBr(001) facet. For this separation, the MSP is -440 mV. The CPD of the tip-surface system has been arbitrarily set to $V_{cpd} = 0$ V.

anion of the KBr surface. At similar height, the MSP of the (001) KBr facet is -440 mV. The choice of that value of z_{min} stems from the exponential decay of the electrostatic short-range force. One has to be close enough to the surface to get a force able to trigger the mode. For that distance, the force yields -52 pN, -35 pN and -46 pN with tips 1, 2 and 3, respectively. This is also why we have set a relatively large value for the bias modulation, although this value can be significantly lowered experimentally owing to longer-range electrostatic forces. For the sake of clarity we have set the CPD of the tip-surface system equal to zero, $V_{cpd} = 0$ V. The DC part of the bias is swept from -5 V to +5 V within 30 s. The values of the local CPDs are reported in table I.

Analytic and numeric curves give qualitatively similar trends, both pointing out the strong influence of the tip geometry on the measured local CPD. Although the asperity radius between tips 1 and 3 merely differ by 10% ($R_a = 1$ and 1.1 Å, respectively), their relative local CPDs are shifted by several volts (1.5 V with the analytic approach and about 3 V for the numeric approach). This stems from the term $F_\mu^{(2)}$ which, in the case of tip 3, is decreased because the mesoscopic part of the tip is 10 pm farther away from the surface than for tip 1. Therefore the influence of the MSP, which decays exponentially fast, onto the tip is weaker. The strength of $F_\mu^{(2)}$ being governed by the coefficient C_2, the above argumentation can be interpreted as if C_2 was strongly lowered between tip 1 and tip 3 (given a value of z_{min}). According to equ.10, this must result in a consistent change of the local CPD. Regarding tip 2, the effect is stronger even as the asperity is bigger than for the two former tips. Furthermore, the mesoscopic part of the tip being bigger, the tip-surface

capacitor is larger, which strengthens the influence of the term $F^{(1)}_{m\mu}$, *i.e.* coefficient C_1 in equ.10. The influence of tip's radii R and R_a on the measured local CPD is discussed in more detail in section V.

A straightforward consequence is that the measured local CPDs neither match the CPD of the tip-surface system (0 volt), nor they are comparable to the MSP at similar distance. The values are systematically much over-estimated (absolute values). This was predicted by the analytical approach and is indeed confirmed numerically. Thus, it is an effect to be considered for interpreting the experiments.

The above elements must not hide the quantitative discrepancies between analytic and numeric curves. First, the analytic approach lacks in providing a value of the local CPD similar to the numerical one and second, the curvature of the curves at large bias differs between the two approaches. Regarding the numeric approach, the differential equations are integrated consistently without approximations. Therefore, we believe that the numeric local CPDs are somewhat reliable. On the contrary, the analytic approach relies on numerous assumptions, some of which being strong (harmonic behavior of the mode). This is why it is possible to derive a simple expression for $V^{(c)}_{DC}$ wherein all the assumptions are actually gathered within coefficients a_0 and b_0, *i.e.* the zero-order Fourier components of the short-range electrostatic force. When tuning them by only few percents, the value of $V^{(c)}_{DC}$ is significantly modified. Furthermore, due to the linearization procedure, the analytic solution for A_1 is basically valid for a small force, *i.e.* in a small region around the CPD value. Therefore, the curvature of the numerical curves is likely connected to the substantial increase of the electrostatic force which modifies the excitation, and consequently the dynamics, of the second eigenmode.

B. FM-KPFM

1. Analytic approach

In FM-KPFM, the bias voltage modulates the electrostatic force and thus, the oscillation of the cantilever is frequency-modulated at $f'_0 + f_{mod}$ and $f'_0 + 2f_{mod}$, as shown in the work by Zerweck *et al.*[25]. f'_0 is the resonance frequency of the cantilever close to the surface, *i.e.* shifted from its natural value f_0 due to the influence of other forces like Van der Waals and

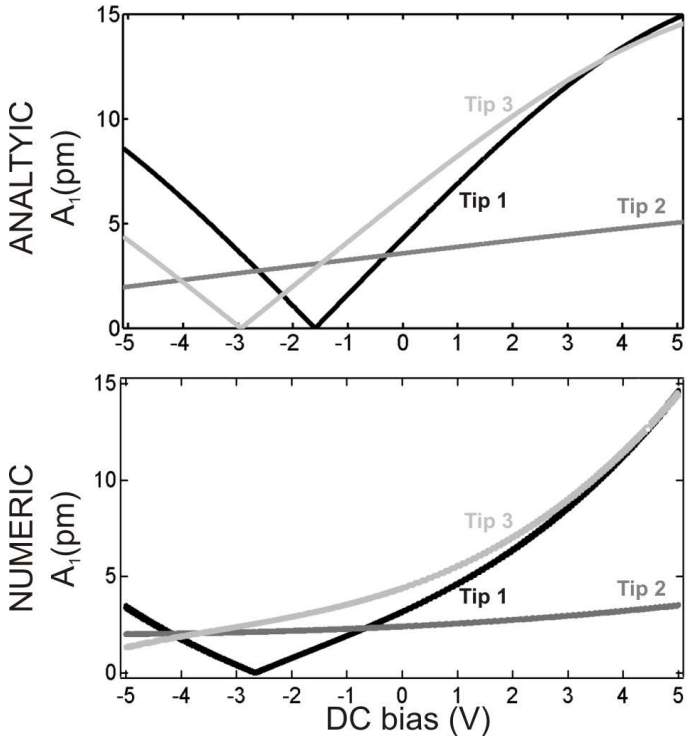

FIG. 3: Analytic and numeric A_1 *vs.* V_{DC} spectroscopic curves computed in AM-KPFM mode at $z_{min} = 3$ Å with the three tips defined in fig.2. The values of the local CPD for tips 1 and 3 are given in table I.

chemical short-range ones, but also the DC part of the electrostatic force. This means that, for a given value of z_{min}, the frequency shift supplied by the PLL is not constant anymore, but modulated at f_{mod} and $2f_{mod}$. It is reminded that in FM-KPFM, f_{mod} is of about 1 kHz and hereby far from any resonance of the cantilever. Therefore, it is also very low compared to f_0' and f_0. In order to derive an analytic expression for Δf, we use the formula introduced by Giessibl[31]. When applied to FM-KPFM, this approximated expression of Δf is very good because, owing to the range of the electrostatic force, the perturbation of the harmonic motion of the first eigenmode of the cantilever is weak (particularly the one due to the AC part), but also because the control electronics is designed to maintain the harmonic motion of the cantilever. We then perform the calculation of Δf by using this formalism coupled to the following quasi-static approximation: because $f_{mod} \ll f_0$, it is assumed that the AC part of the electrostatic force is constant during one oscillation cycle of the cantilever. In ref.[16], Krok *et al.* have used a similar approach with a different expression for the electrostatic force, however scaling similarly with V_b. Hence:

$$\begin{aligned}
&\Delta f = \tfrac{f_0}{2k_0A_0} e^{-\alpha z_{min}} \{ \\
&\Big[C_1(V_{DC} - V_{cpd})a_1 + b_1 e^{-\alpha z_{min}} [C_0 + C_2(\tfrac{V_{mod}^2}{2} + (V_{DC} - V_{cpd})^2)] \Big] + \\
&[C_1 a_1 + 2(V_{DC} - V_{cpd}) C_2 b_1 e^{-\alpha z_{min}})]\, V_{mod} \cos(2\pi f_{mod} t) + \\
&[C_2 b_1 e^{-\alpha z_{min}}]\, \tfrac{V_{mod}^2}{2} \cos(4\pi f_{mod} t) \Big\}
\end{aligned} \tag{11}$$

a_1 and b_1 are now the f_0-Fourier components (first components) of the exponential functions discussed above. The first term in equ.11 is static and gives, for $V_{mod} = 0$, the parabolic spectroscopic response at each point over the surface. The other terms describe the dynamic Δf variations occurring when scanning the surface. Considering the case of spectroscopic curves, the maximum of the Δf *vs.* V_{DC} curve is reached when:

$$V_{DC}^{(c)} = \left.\frac{\partial \Delta f}{\partial V_{DC}}\right|_{V_{mod}=0} = 0 \rightarrow V_{DC}^{(c)} = V_{cpd} - \frac{C_1}{2C_2}\frac{a_1}{b_1} e^{+\alpha z_{min}} \tag{12}$$

Hence, the value of the compensated CPD in FM-KPFM is almost similar to the one measured in AM-KPFM. The difference stems from the ratios a_0/b_0 and a_1/b_1. Expressions 10 and 12 show that the compensated CPD in AM-KPFM is sensitive to the averaged value of the electrostatic force (0-order Fourier component of the force), whereas it is sensitive to its Fourier component at the vibration frequency of the fundamental eigenmode in FM-KPFM. To some extend, this illustrates the long-standing idea that AM-KPFM is sensitive to the electrostatic force and that FM-KPFM rather to its gradient[32]. Coefficients a_n and b_n only depend on the vibration amplitude of the fundamental eigenmode, A_0. However, for $n = 0$ and 1, they weakly depend on it as soon as A_0 is larger than a few nanometers. With $A_0 = 4$ nm, one has $a_0 = 0.1155$, $a_1 = 0.1080$ and $b_0 = 0.0724$, $b_1 = 0.0766$. Hence FM- and AM-KPFM will not provide similar values for the local CPD, but they will neither differ significantly.

2. Numeric approach

The numeric implementation of the FM-KPFM setup is easier than the AM-KPFM one as the modulated signal is provided by the PLL without further processing. However, the sequence of the calculation of the spectroscopy curve slightly differs from the AM-KPFM one. The first part of the calculation is similar. When the approach is complete, we set

$V_{mod} = 0$, consistently with what is done during the experiments. Then, the DC part of the bias is swept. Similar sets of parameters have been used.

3. Results and discussion

Analytic and numeric Δf *vs.* V_{DC} spectroscopic curves are reported in fig.4. For that set of simulations, we have used $f_{mod} = 2.5$ kHz. The values of the local CPDs are reported in table I. As stated in the former section, the analytic values of the CPD slightly differ from those deduced by AM-KPFM. Similar trends are observed for the numerical results. The qualitative behavior between analytic and numeric curves is also similar, the measured local CPD with tip 2 being much shifted compared to the one measured with tips 1 and 3. Again, the local CPD's neither reflect the CPD of the tip-surface system, nor the MSP at similar separation.

Finally, we would like to point out the following issue. Although the analytic variations of Δf exhibit a quadratic dependence with V_{DC}, readily visible in equ.11, it is impossible to fit the numerical variations with a quadratic polynom of V_{DC} to a good accuracy (*cf.* fig.4). So far, this behavior remains not understood. Although numerous attempts, including careful investigations of the influence of the PLL, we did not manage to identify the origin of this effect. It is obviously possible to fit the Δf variations with a better accuracy when using higher-order polynoms, but this does not answer the question of the origin of such power laws, which do not stem from the expression of the electrostatic force.

V. OVERALL GEOMETRICAL INFLUENCE OF THE TIP TO THE LOCAL CPD: CONNEXION WITH LONG-RANGE ELECTROSTATIC FORCES

A. Influence of the tip apex structure

The above elements have demonstrated that the compensated local CPD was strongly sensitive to the tip's apex geometry (radii R and R_a). In order to assess how strong this dependence is, we have used equ.12 (FM-KPFM case) to plot the variations of the local CPD *vs.* R and R_a at constant height (*cf.* fig.5a). This is only made possible analytically, although the analytic method is less accurate than the numeric one. The parameters are

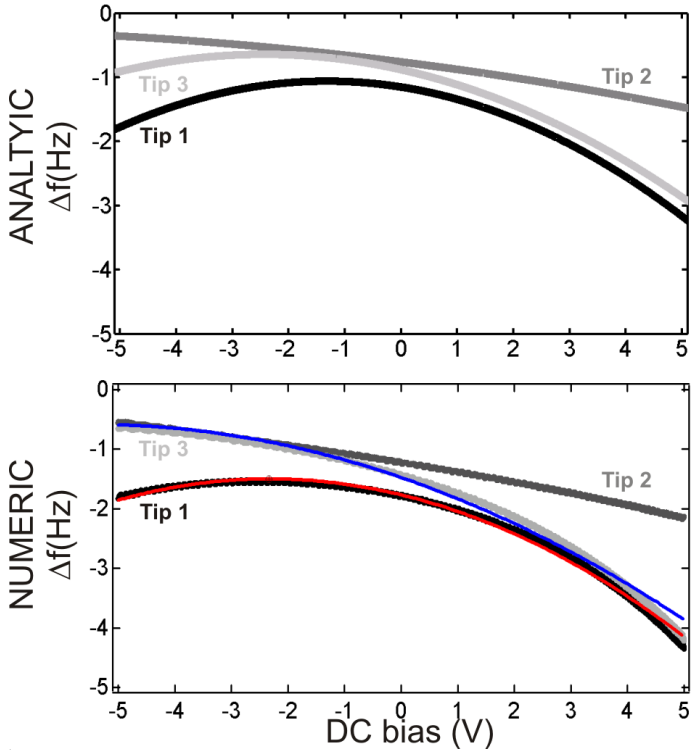

FIG. 4: Analytic and numeric Δf *vs.* V_{DC} spectroscopic curves computed in FM-KPFM mode at $z_{min} = 3$ Å with the three tips defined in fig.2. The values of the local CPD for tips 1 and 3 are given in table I. For these tips, quadratic fits have been performed (continuous red and blue curves, respectively), which do not fit the numerical variations to a good accuracy (*cf.* text).

identical to those given before, in particular $z_{min} = 3$ Å on top of an anion. The mesoscopic radius R is varied from 3 to 15 nm and R_a from 1 to 1.6 Å. It is not allowed to make R_a bigger owing to the main assumption of the model $R_a \ll R$. Despite the rather narrow range of R_a, the local CPD is strongly decreased from -1.3 V (*cf.* also table I) down to -9 V as R_a gets bigger. It is not possible to provide a tractable expression of the local CPD with R_a owing to its complex and implicit dependencies (coefficients D_1 and A_2). However, some keys for understanding this behavior have been given in section IV A. On the opposite, the CPD does not exhibit a noticeable dependence with R, meaning that the nano-asperity plays a key role in the occurrence of the high-resolution imaging in KPFM.

B. Influence of long-range capacitive forces

So far, we have been concerned about the influence of the electrostatic force stemming from the mesoscopic/microscopic structure of the tip on the measured local CPD, without taking into account long-range capacitive forces. Nevertheless, on the experimental level, these forces are always present. Furthermore equs.10 and 12 exhibit a surprising exponential dependence of the local CPD with the tip-surface separation, which should lead to a divergence/saturation of the measurement when attempting to perform it far from the surface.

In order to extend the present framework, the influence of a long-range capacitive force on the measured local CPD has been assessed. We stick to the geometry defined before: the counter-electrode, the bulk dielectric and the tip on top of it, but we consider an additional macroscopic metallic electrode placed a few microns above the tip[33], hence several millimeters away from the counter-electrode. The electrode itself has millimetric dimensions and is at the same potential than the tip, V_b. It depicts, to some extend, the cantilever and the tip holder when mounted in the microscope. With such a configuration, since the MSP decays exponentially with the tip-surface separation, it does not influence this electrode. Therefore, on the electrostatic level, the "mesoscopic/microscopic" problem and the "macroscopic" problem are rather decoupled, which is equivalent to include an additional long-range component to the total electrostatic force. Hence, equ.4 is modified into:

$$F_{es}(V_b, z) = F_{m\mu}^{(1)} + F_{\mu}^{(2)} + F_M, \tag{13}$$

To derive an approximate expression of F_M, let's consider (1)-a planar capacitor with surface $\mathcal{S}$ and a distance between electrodes z_M corresponding to several millimeters and (2)-that the dielectric sample fills entirely the vacuum between the electrodes. The condition 1 actually implies to neglect z, which is of the order of a few angströms, with respect to z_M each time it is necessary. Then, we get:

$$F_M(V_b, z) \simeq -\frac{C_2'}{(z_M + z)^2}(V_b(t) - V_{cpd})^2, \tag{14}$$

with $C_2' = \epsilon_0 \widetilde{\epsilon}_d^2 \mathcal{S}/2$. A quick estimate for $\mathcal{S} = 1$ mm^2, $z_M = 5$ mm ($C_2' = 8.5\ 10^{-5}$ pN.m^2.V^{-2}) and $V_b = 1$ V yields $F_M \simeq -3$ pN.

For the FM-KPFM case, when applying Giessibl's formalism, an analytical expression for the frequency shift connected to F_M can be derived. When applying a similar procedure than the one used to derive equ.12 to the frequency shift resulting from the total force (equ.13), the expression of the compensated CPD now becomes:

$$V_{DC}^{(c)} = V_{cpd} - \frac{C_1 a_1 e^{-\alpha z_{min}}}{2C_2 b_1 e^{-2\alpha z_{min}} + 4\pi C_2' A_0 / z_M^3} \tag{15}$$

It is reminded that A_0 is the vibration amplitude of the first cantilever eigenmode. The graph of $V_{DC}^{(c)}$ *vs.* z_{min} is reported in fig.5b for tips 1, 2 and 3. The diverging behavior predicted by equs.10 and 12 has disappeared because the term carrying the exponential decay in the denominator (deriving from $F_\mu^{(2)}$) is now compensated by the long-range one. Therefore, the decaying exponential in the numerator (deriving from $F_{m\mu}^{(1)}$) nullifies the local CPD far from the surface. This behavior is more likely to be measured and intricately originates from long-range electrostatic, macroscopic, interactions. The shape of the curve looks like the resonance curve of a harmonic oscillator. Hence, there is an optimum tip-surface separation for which, the strength of the KPFM contrast will be enhanced, although the measured value will not be correlated to the MSP. Upon the tip geometry, the maximum of the curve occurs at various tip-surface separations. In particular, the discrepancies between tips 1 and 2 suggest that it is more likely to achieve a stabler KPFM imaging regime with tips including a not too big mesoscopic apex. Let us notice that such a behavior is expected to stand also for the AM-KPFM case owing to the analogy between equs.10 and 12.

At last, we are aware that the predicted variations of the compensated local CPD are very large. This is the consequence of the power laws occurring in the expression of the short-range electrostatic force, themselves deriving from the raw geometry of the tip. That large variations will never be measured on the experimental level owing to realistic tip shapes which differ significantly from the one of our model. Nevertheless, we still believe that the reported variations are qualitatively relevant.

VI. CONCLUSION

The influence of short-range electrostatic forces on the measured local CPD by means of AM- and FM-KPFM methods has been discussed. The sample is a bulk alkali halide single crystal. This work relies on numeric and analytic descriptions of both KPFM modes. The

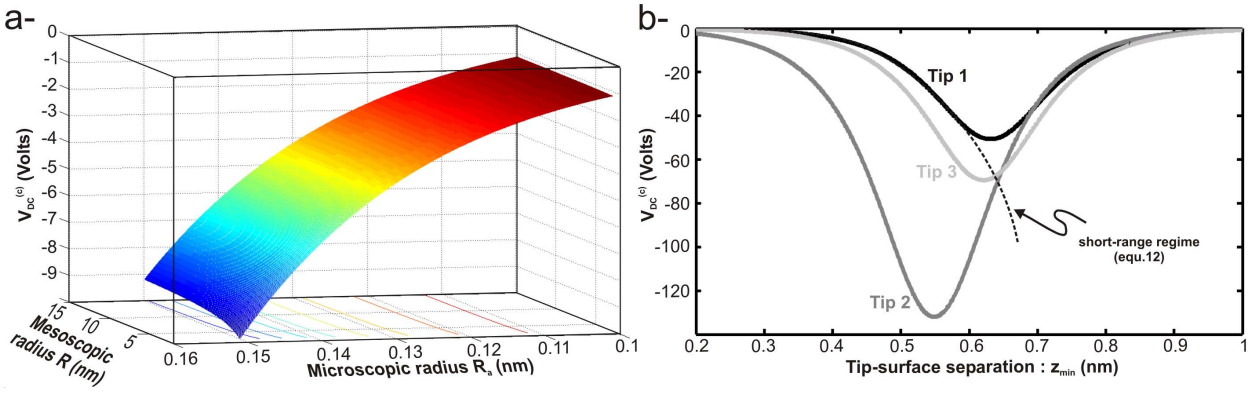

FIG. 5: a- Evolution of the compensated local CPD as a function of tip's radii R and R_a computed from equ.12, *i.e.* for the FM-KPFM case. A strong R_a dependence is noticed. b- Compensated local CPD *vs.* tip-surface separation computed from equ.15 for tips 1 (black), 2 (dark grey) and 3 (light grey). The diverging behavior initially predicted when only considering short-range electrostatic forces is now disappeared. Instead, a resonant behavior is observed.

analytic expression for the short-range electrostatic force is derived from a previous work and exhibits a short-range distance dependance and a linear as well as quadratic dependence of the bias voltage. The linear term is responsible for the atomic-scale CPD contrast, while the quadratic one accounts for the detected signal by the KPFM methods. The latter term stems from the dynamic polarisation of the ions of the crystal. Analytic and numeric approaches stress the influence of the linear term on the measured compensated CPD which makes it deviating not only from the actual value of the CPD, but also from the surface potential. Hence, in the short-range regime, the AM- or FM-KPFM compensated local CPD neither reflects the tip-surface CPD nor the local surface potential, but rather an effective value which is convoluted by the geometry of the tip. Nevertheless, it is shown that the lateral periodicity of the signal is preserved, which makes the AM- or FM-KPFM methods indeed sensitive to atomic scale changes of the surface potential, as demonstrated experimentally, although quantitative numbers are unlikely derivable.

It has also been found that the local CPD detected by means of AM- or FM-KPFM is expected to differ. This stems from the detection methods which are not performed at similar frequencies, hence selecting different Fourier components of the modulated force for the signal processing. However, when using large amplitudes like those regularly used in beam-deflection based nc-AFM (a few nm), this effect is expected to be weak.

Finally, the influence of long-range, capacitive, electrostatic forces has been addressed in conjunction with the short-range ones. The local CPD then exhibits kind of a resonance peak as a function of the tip-surface separation. The position of the peak depends on the tip geometry, but is expected to occur at a few angströms above the surface. The occurrence of a resonance phenomenon illustrates the idea that there is an optimum tip-surface separation for achieving a large vertical KPFM contrast, although this contrast is not correlated to the surface potential.

---

[1] J. Weaver and D. Abraham, J. Vac. Sci. Technol. B **9**, 1559 (1991).

[2] S. Sadewasser and M. Lux-Steiner, Phys. Rev. Lett. **91**, 266101 (2003).

[3] S. Sadewasser, P. Carl, T. Glatzel, and M. C. Lux-Steiner, Nanotechnology **15**, S14 (2004).

[4] C. Barth and C. Henry, Nanotechnology **17**, S155 (2006).

[5] The measured CPD is positive when the bias voltage is applied to the sample, negative otherwise.

[6] C. Sommerhalter *et al.*, Appl. Phys. Lett. **75**, 286 (1999).

[7] A. Kikukawa, S. Hosaka, and R. Imura, Rev. Sci. Instrum. **67**, 1463 (1996).

[8] S. Kitamura and M. Iwatsuki, Appl. Phys. Lett. **72**, 3154 (1998).

[9] K. Okamoto, K. Yoshimoto, Y. Sugawara, and S. Morita, Appl. Surf. Sci. **210**, 128 (2003).

[10] Y. Rosenwaks, R. Shikler, T. Glatzel, and S. Sadewasser, Phys. Rev. B **70**, 085320 (2004).

[11] H. Hoppe *et al.*, Nanoletters **5**, 269 (2004).

[12] S. Kitamura, K. Suzuki, and M. Iwatsuki, Appl. Sur. Sci. **140**, 265 (1999).

[13] Y. Sugawara, T. Uchihashi, M. Abe, and S. Morita, Appl. Surf. Sci. **140**, 371 (1999).

[14] S. Kitamura, K. Suzuki, M. Iwatsuki, and C. B. Mooney, Appl. Surf. Sci. **157**, 222 (2000).

[15] K. Okamoto, Y. Sugawara, and S. Morita, Jpn. J. Appl. Phys. **42**, 71637168 (2003).

[16] F. Krok *et al.*, Phys. Rev. B **77**, 235427 (2008).

[17] A. Sasahara, C. L. Pang, and H. Onishi, J. Phys. Chem. B **110**, 13453 (2006).

[18] G. Enevoldsen *et al.*, Phys. Rev. Lett. **100**, 236104 (2008).

[19] F. Bocquet, L. Nony, C. Loppacher, and T. Glatzel, Phys. Rev. B **78**, 035410 (2008).

[20] K. Wandelt, Appl. Surf. Sci. **111**, 1 (1997).

[21] C. Leendertz, F. Streicher, M. C. Lux-Steiner, and S. Sadewasser, Appl. Phys. Lett. **89**, 113120 (2006).

[22] L. Nony *et al.*, Phys. Rev. B **74**, 235439 (2006).

[23] S. Hudlet, M. Saint-Jean, C. Guthmann, and J. Berger, Eur. Phys. J. B **2**, 5 (1998).

[24] M. Guggisberg *et al.*, Phys. Rev. B **61**, 11151 (2000).

[25] U. Zerweck *et al.*, Phys. Rev. B **71**, 125424 (2005).

[26] C. Sommerhalter *et al.*, Appl. Surf. Sci. **157**, 263 (2000).

[27] O. Sahin, C. Quate, O. Solgaard, and A. Atalar, Phys. Rev. B **69**, 165416 (2004).

[28] C. Loppacher *et al.*, Appl. Surf. Sci. **140**, 287 (1999).

[29] R. Watson, J. Davenport, M. Perlam, and T. Sham., Phys. Rev. B **24**, 1791 (1981).

[30] An opposite behavior would be observed on top of a cation.

[31] F. Giessibl, Phys. Rev. B **56**, 16010 (1997).

[32] T. Glatzel, S. Sadewasser, and M. Lux-Steiner, Appl. Surf. Sci. **210**, 84 (2003).

[33] Usual silicon-based commercial cantilevers have integrated tips with 10 microns height.

Appendix

Out of ref.19, the coefficients l_0, l_1, l_2 and l_3 can be written:

$$l_0 = \frac{C_1 a_0}{m_1} e^{-\alpha z_{min}} V_{mod} + 2\frac{C_2 b_0}{m_1} e^{-2\alpha z_{min}} (V_{DC} - V_{cpd}) V_{mod} \tag{16}$$

$$l_1 = \frac{\omega_1^2}{Q_1} \tag{17}$$

$$l_2 = -\frac{2\alpha C_0}{m_1} b_0 e^{-2\alpha z_{min}} - \frac{\alpha C_1}{m_1} a_0 e^{-\alpha z_{min}} (V_{DC} - V_{cpd}) - \frac{2\alpha C_2}{m_1} b_0 e^{-2\alpha z_{min}} \left[(V_{DC} - V_{cpd})^2 + \frac{V_{mod}^2}{2} \right] \tag{18}$$

$$l_3 = -\frac{2\alpha C_2}{m_1} b_0 e^{-2\alpha z_{min}} \frac{V_{mod}^2}{4} \tag{19}$$